Progress on HTS Undulator Prototype Coils for Compact FEL Designs

S. C. Richter, A. Ballarino, D. Schoerling, T. H. Nes, A. Bernhard, and A.-S. Müller

***Abstract*—Compact free-electron lasers require short accelerator structures followed by high peak field and short-period undulators to produce coherent radiation up to hard X-rays. Likewise, future lepton colliders, like CLIC or FCC-ee, require high-field damping wigglers for the creation of low emittance beams. The application of high-temperature superconductor (HTS) in the form of coated REBCO tape to undulators and wigglers enables higher magnetic fields and larger operating margins. This paper discusses the potential of HTS for a superconducting vertical racetrack (VR) undulator coil geometry as well as results of the development work done on a prototype coil, with a period length of 13 mm, wound from coated REBCO tape conductor. Design and assembly aspects as well as first results from powering tests at 77 K are presented and discussed.**

***Index Terms*—Free electron lasers, high-temperature superconductors, superconducting devices, undulators.**

I. Introduction

THE next generation of compact free electron lasers needs undulators with high magnetic peak fields and short period lengths. These characteristics are crucial to emit laser radiation in the hard X-ray regime. The European Union funded CompactLight (XLS) design study, to which CERN and the Karlsruhe Institute of Technology (KIT) contribute, investigates various approaches to achieve such a compact design [1]. The latest proposal for hard X-rays is based on undulators with a magnetic peak field greater than 1 T and a period length of 13 mm.

Likewise, future lepton colliders studied at CERN, e.g., CLIC (Compact Linear Collider) and FCC-ee (Future Circular Collider), have a need for damping wigglers with high magnetic peak fields to create low emittance beams [2], [3]. CLIC aims for wigglers with a peak field on the beam axis of 3 T with around 50 mm period length. A niobium-titanium (Nb-Ti) prototype wiggler with a magnetic gap of 17 mm already operates in the synchrotron KARA at KIT [4].

This work was supported by The Wolfgang Gentner Program of the German Federal Ministry of Education and Research and the DFG-funded Doctoral School, Karlsruhe School of Elementary and Astroparticle Physics: Science and Technology. *(Corresponding author: Sebastian C. Richter.)*

S. C. Richter is with the Conseil européen pour la recherche nucléaire (CERN), 1211 Geneva, Switzerland, and also with the Karlsruhe Institute of Technology (KIT), 76131 Karlsruhe, Germany (e-mail: sebastian.richter@cern.ch).

A. Ballarino, D. Schoerling, and T. H. Nes are with the Conseil européen pour la recherche nucléaire (CERN), 1211 Geneva, Switzerland.

A. Bernhard and A.-S. Müller are with the Karlsruhe Institute of Technology (KIT), 76344 Karlsruhe, Germany.

At present, superconducting insertion devices, like wigglers and undulators, are mainly built from Nb-Ti, a low temperature superconductor (LTS) with a critical temperature below 10 K, usually operated in liquid helium. The characteristic of high-temperature superconductors (HTS), here REBCO (rare-earth barium copper oxide), is to stay superconductive under high external fields (e.g., YBCO: $B_{c2,\perp}(4.2\ \mathrm{K}) \approx 100\ \mathrm{T}$) at low ($<$ 30 K) temperatures [5], [6]. Stand-alone solenoids wound from REBCO tape reached magnetic fields in the conductor of 16.5 T at 23 K [7] and more in lower temperatures [8], showing the material's potential of operating with engineering current densities of 1 kA/mm^2 at 20 T and 23 K. The protection of a magnet for these high current densities is still an issue, e.g., in a quench event. We approach this by choosing a non-insulated (NI) design, where the current is able to bypass normal zones by circulating radially inside the coil.

Another NI and partial insulated study was performed by I. Kesgin *et al.* [9]. The latter improved the current redistribution during ramp up. They also presented a novel continuous winding scheme for an undulator period $\lambda_\mathrm{u} = 16$ mm. However, this scheme might be hard to adapt to smaller periods using 4 mm wide tape and quench protection was challenging.

Further early HTS undulator studies investigated stacked REBCO tapes [10], insulated coils [11] or bulk staggered arrays [12]. All aimed to demonstrate that higher magnetic peak fields on undulators' beam axis may become possible thanks to HTS. Additionally, the temperature margin may facilitate the operation compared to the state-of-the-art LTS technology, and higher operating temperatures become feasible (e.g., lower costs, cryocoolers). These benefits may make HTS a superior material for designing future high-field superconducting undulators and wigglers.

In a collaboration between the KIT, Germany, and CERN, Switzerland, we are investigating horizontal racetrack, vertical racetrack (VR) and helical coils optimized for the use in undulators and wound from coated REBCO tape conductor. For each feasible design, we plan to build prototype coils which will be evaluated by their performance. In this paper we report on the progress of the work done on the HTS VR prototype coils, which are sketched as a VR short model in Fig. 1.

II. VR Undulator Coil Design

Aiming for an application field in XLS and having performed a 2D electro-magnetic parameter space investigation [13], [14], a configuration with an undulator period length $\lambda_\mathrm{u} = 13$ mm and a magnetic gap of 6 mm has been selected for the prototype coil. As displayed in Fig. 2, the VR coil was chosen to have a specific D-shape with a straight section facing the beam pipe and an iron core. Here, $\lambda_\mathrm{u}/2$ consists of 4 mm wide coated REBCO

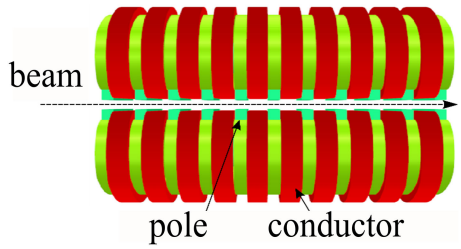

Fig. 1. 3D sketch of a five period short model of the investigated vertical racetrack (VR) undulator geometry with iron poles (side view).

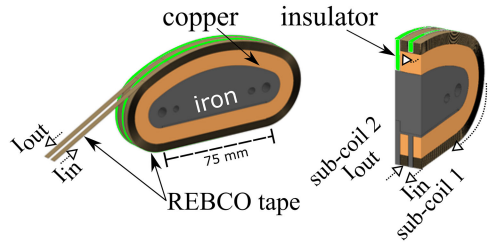

Fig. 2. 3D geometry of the VR undulator coil. Left: full coil with copper and iron bodies. Right: Cross-section showing the two VR sub-coils 1 and 2 and the current path (indices: in/out) dashed arrows, respectively. Copper (orange), iron (grey) and G11 (green) parts are colored, respectively.

conductor and a pole width of 2.5 mm (iron and its insulation), thus $J_e \cong J_w$.

The VR coil design consists of two NI sub-coils forming a full undulator period by having the current flowing in opposite direction. The innermost turns of both sub-coils are soldered along the curved side of their D-shape to a 10 mm wide coated REBCO tape, the c-tape that connects them electrically. The current enters sub-coil 1 and goes all the way into its center. Via the c-tape the current is then brought to the innermost turn of sub-coil 2. Here, a copper winding body serves as additional stabilizer on the inside. The current exits the VR coil through sub-coil 2. Both coils are wound with their innermost layer on the same copper body. All other turns are separated by insulator plates. The iron poles are connected to a solid iron core, which is located inside the copper body.

A. 3D Electro-Magnetic Modelling

We performed electro-magnetic investigations using Opera [15]. The critical surface of REBCO conductors was based on fits done at CERN [16], [17]. The critical current density J_c was defined by considering the worst case scenario: the maximum B-field on the conductor $\mathbf{B_{cond}}$ perpendicular to the tape plane. This showed to be a sufficient assumption as we found $\mathbf{B}_\perp = 99.95\%\ \mathbf{B_{cond}}$ at 4.2 K. The VR coil model was investigated for an operating temperature of 4.2 K to reach highest fields and forces. For the Bruker HTS tape, used for the prototype coil, we found J_e(4.2 K, $B_\perp = 4.9$ T) $= 2071$ A/mm^2. Published experimental results [9] support the outcome of our simulations for REBCO conductors. Operation in liquid nitrogen (LN2) at 77 K was likewise simulated. Significant values for both operating temperatures can be found in Table I.

The maximum $\mathbf{B_{cond}}$ and the Lorentz forces were investigated for J_e(4.2 K). The latter were then linked to the mechanical analysis to calculate the mechanical stresses. The maximum computed $\mathbf{B_{cond}}$ for VR was found to be 4.9 T on the facing coil

TABLE I
SIMULATED VR UNDULATOR COIL PARAMETERS FOR BRUKER HTS TAPE

Operating values	VR coil (4.2 K)	VR coil (77 K)
Undulator period λ_u	13 mm	
Coil pack cross-section	4 mm x 5 mm	
Min. conductor bending radius	20 mm	
Current density J_{op} (= 90% J_c)	1864 A/mm^2	67.5 A/mm^2
Current per tape I_{op} (= 90% I_c)	735 A	27 A
Stored energy	103.9 J	0.25 J
Inductance	384.7 µH	679.0 µH
Max. B-field at conductor $\boldsymbol{B}_{\mathbf{cond}}$	4.4 T	0.6 T
Peak B-field on beam axis $\boldsymbol{B}_y$	1.5 T	0.16 T

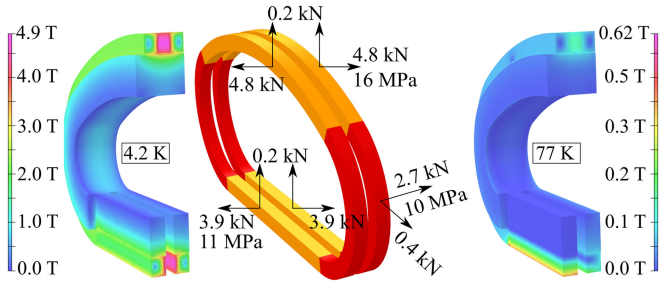

Fig. 3. Left: VR coil field calculation for J_e (4.2 K) = 2071 A/mm^2 (conductor and copper only). Center: Lorentz forces on the VR coil pack at 4.2 K (conductor only). Right: VR coil field estimation for J_e (77 K) = 75 A/mm^2.

sides. Here, maximum forces on the conductor pack were 4.8 kN. Distributed over a conductor segment (same curvature), the maximum pressure was 16 MPa, facing sideways. While the iron poles do increase the magnetic field on the beam axis, the iron core keeps the Lorentz forces perpendicular to the REBCO tape's surface at max. 400 N. Results from simulations are illustrated in Fig. 3.

B. Mechanical Modelling

ANSYS Workbench [18] was used to calculate the stress and strain on the VR coil during cool-down from room temperature to 4.2 K and during powering with a J_e of 2071 A/mm^2. The latter was obtained from 3D magnetic simulations as described in the section above and imported into the mechanical model as element force density. The mechanically investigated VR coil was modelled taking into account the materials' properties. The Bruker HTS tape was modelled as homogenous material composed of 100 μm stainless steel, 40 μm copper, 7 μm silver and 3 μm yttrium. In order to investigate the caused stress and strain, all connecting materials have been defined as bonded contacts.

Values of the equivalent (von-Mises) stress have shown to stay below the tolerable thresholds, i.e., maximum local stresses of 64 MPa were observed on the tape conductor pack [19]. The mechanical design includes a supporting structure to avoid any REBCO tape movement or deformation.

C. Heat Load Estimation

Heat dissipation in the cryogenic environment shall be minimized, here with regard to a full-size undulator. The main contribution for superconducting undulators are the electrical joints. For operating an undulator, a total feasible cooling power

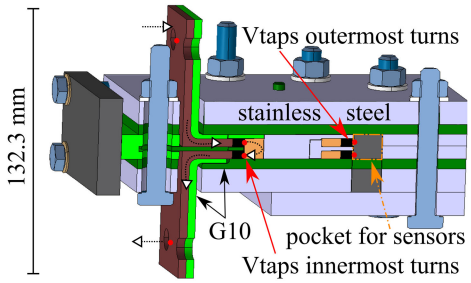

Fig. 4. Cross-section through the 3D geometry of the VR undulator coil mounted in its support structure. Red points display the position of the Vtaps. Dashed arrows symbolize the current flow through the assembly.

of 2 W/m from cryocoolers was estimated at 4.2 K (based on experience at KARA, KIT) [20].

Consequently a period length of 13 mm leads to a threshold value of 2 W/m · 13 mm = 26 mW per period with two VR coils (full model), thus 13 mW for one VR coil, in our case. The joint surface on the connecting c-tape for one sub-coil was therefore calculated to be $A_{\mathrm{JointC}} = 9.53\ \mathrm{cm}^2$. The straight length was chosen to be 75 mm to ensure a sufficiently large surface on the curved sides of the VR coil. A joint resistance $R_{\mathrm{Joint}}(4.2\ \mathrm{K}) = 36\ \mathrm{n\Omega\ cm}^2$ is assumed when soldering face-to-face with the superconducting layers [21]. With the calculated $I_{\mathrm{op}}(4.2\ \mathrm{K}) = 735$ A we get

$$P = {I_{\mathrm{op}}}^2\,(4.2\,\mathrm{K}) \cdot \left(R_{\mathrm{Joint}}\,(4.2\,\mathrm{K})\,/A_{\mathrm{JointC}}\right) = 2.04\,\mathrm{mW}\ . \quad (1)$$

For the two sub-coils this gives a total value of 4.08 mW and leaves margin for incoming and outgoing joints to copper terminals or neighboring coils when being stacked to a full-size undulator with hundreds of periods.

III. VR Undulator Coil Manufacturing

The VR coil was manufactured by winding two NI sub-coils with 4 mm wide and 100 µm thick Bruker HTS tape with a REBCO layer as superconductor. The two sub-coils were wound simultaneously with the same direction on the copper winding body. The superconducting layer faced inside, i.e., the copper body, to have the REBCO under compression. The winding tension was constantly controlled and kept at 30 N. The first turn of each tape was soldered along the curved side to the c-tape and fixed by a stainless steel pin to the copper body (see Fig. 5a). The soldering with Sn62Pb36Ag2 solder paste was done after the first turn was wound by heating the VR coil up to 185 °C for 5 min. Voltage taps (Vtaps) were placed in these joints. Insulation sheets were mounted to cover the side walls of the stacks. The winding continued until each tape stack had reached a thickness of 5 mm, giving a $4\times5\ \mathrm{mm}^2$ conductor cross section (Fig. 5c). This required 51 turns.

For the last turn, the two Bruker HTS tapes were soldered to their penultimate turn along the curved sides by using 97In3Ag solder paste. The VR coil was heated up to 155 °C for 5 min. The final VR coil after the winding process is presented in Fig. 5e.

After winding, the VR coil was mounted in its stainless steel supporting structure. G10 and Kapton were used as insulating materials. A copper lead was pressed on the curved side of each sub-coil, as shown in Fig. 5d to g. To increase the quality of the connection, a thin indium foil was placed in between the copper lead and the VR coil. A contact pressure of around 5 MPa was

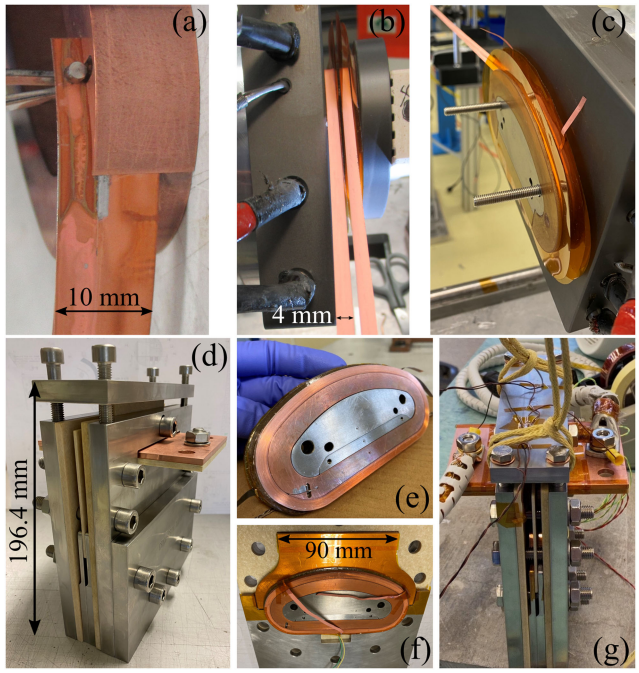

Fig. 5. (a) A close-up of the pin to fix start of the winding. (b) VR coil winding process with two 4 mm wide Bruker HTS tapes being wound in parallel. (c) VR coil with emerging Vtaps. (d) Assembled support structure. (e) VR coil before mounting in the support structure. (f) Copper lead placement. (g) VR coil fully mounted, all six Vtaps connected and ready for testing. The resistance over the entire assembly with Cu leads was measured to be 340 mΩ at 293 K.

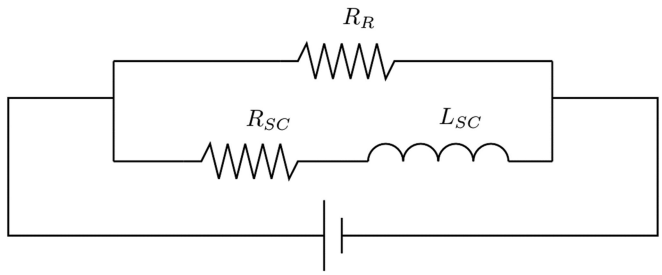

Fig. 6. Electrical circuit diagram representing a non-insulated (NI) coil with one turn. The resistive path with inductance is neglected. For each turn, the current can choose between the resistive (R) radial path and the superconducting path (SC) including an inductance L. $R_{\mathrm{SC}} = 0\ \Omega$ when $\mathrm{T} \leq \mathrm{T_c}$.

applied by tensioning the four M8 bolts on the top plate. Spring washers were included to prevent a decrease of the clamping pressure due to thermal shrinking.

Overall, six Vtaps and two temperature sensors were placed on the VR coil as marked in Fig. 4. A temperature sensor (PT1000) was attached next to the Vtaps on the outer turns on each sub-coil.

IV. Experimental Results and Discussion

The VR coil discussed in this paper was chosen to be a non-insulated coil to release the quench protection requirements. Below the critical temperature and during transients, the current always has two options in our design: following the superconductive path without any resistance but inductance, or taking the radial path across the tapes with a resistance. This is displayed for a single turn in Fig. 6. Via the Vtaps we monitored the voltage

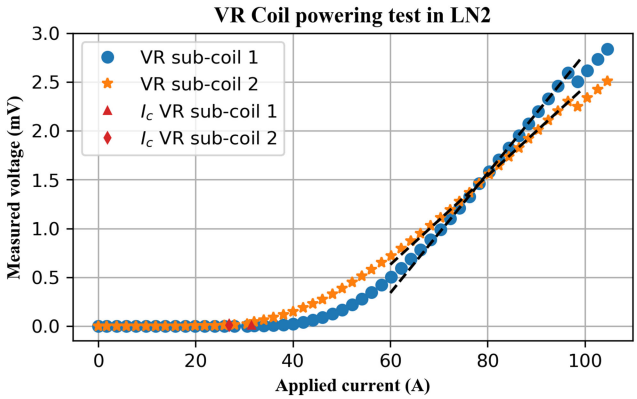

Fig. 7. Measured voltage over each sub-coil, respectively, for stepping up the current to 104 A. After each step of 2 A the current was kept constant for 240 s before the next step. The dashed lines represent the linear fit (saturated radial resistance). Values have been corrected to Vtap resistances.

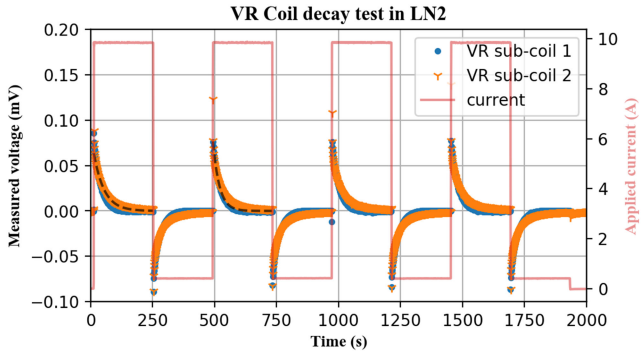

Fig. 8. Voltage decays of both sub-coils for a 0.5 A to 10 A step function. The exponential fits are marked by dashed lines, respectively. One can see a faster decay in sub-coil 2. Values have been corrected to Vtap resistances.

over each sub-coil as well as over the connecting REBCO c-tape, the VR coil and the total assembly.

After the cool down with LN2, we started our tests at 77 K with a current ramping of 0.05 A/s until we could measure a drift in voltage initially over sub-coil 2 (see Fig. 7). The critical current I_c of a sub-coil was defined as last current for which we still measured a resistance of 0 Ω during the ramp up. All higher current values would lead to a finite measureable resistance. Since the VR coil is not symmetric, we expected sub-coil 2 to reach its critical current faster. This is assumed to be due to a higher B-field on the conductor (Fig. 3).

The critical current was measured at $I_{c,s2} = 27$ A in sub-coil 2 and at $I_{c,s1} = 31.5$ A in sub-coil 1. Here, $I_{c,s2}$ is 10% smaller than our calculations predicted, whereas $I_{c,s1}$ is 5% higher. The smaller value of $I_{c,s2}$ might have been caused by local damage of the tape (during winding) and will be further investigated by testing more VR coils. When ramping up the current further, both coils showed a resistive behavior. Each turn after turn was filled up to its individual critical current, at which the extra current is forced to flow radially across the tape. Thus, the V-I curve heads for showing the radial resistance of each sub-coil expressed by its linear slope. Radial resistances across all tapes $R_{R,s1} = 61.3$ μΩ and $R_{R,s2} = 45.5$ μΩ were measured at 77 K for sub-coil 1 and 2, respectively. The difference between the two values is mainly attributed to irregularities in the winding process (e.g., different contact resistances between tapes). A measurement of a second VR coil might reveal more details.

This powering test successfully showed that it was possible to power the VR coil up to ∼400% of the tape's operating current with no degradation of the coil. For coils wound with electrically insulated tapes, temperatures of >300 K would have been reached after ∼0.6 s at 77 K. In the tested NI configuration, current exceeding I_c flowed radially. However, this creates heating (up to 1.2 W) which must be adsorbed by the cryogenic system.

To determine the effective time constants of each sub-coil, the voltage was measured while applying a current following a step function with plateaus at 10 A (Fig. 8).

As shown in Fig. 6, the voltage U can be described as

$$U = (I_{SC} - I_R) \cdot R + L \cdot \mathrm{d}I_{SC}/\mathrm{d}t. \quad (2)$$

When U → 0 V, this can be formed into a differential equation for the current which is given with known solution:

$$\mathrm{d}I_{SC}/\mathrm{d}t = (I_R - I_{SC}) \cdot \mathrm{R/L} \quad \Rightarrow \quad I(t) = I \cdot \mathrm{e}^{-t/\tau}. \quad (3)$$

The voltage decay can be described analog to the current as

$$U = a \cdot e^{-t/\tau}, \text{with, } \tau = L/R \text{ and } a = \text{const.} . \quad (4)$$

By means of the exponential function in (4) we could measure the effective time constants: $\tau_{s1} = 26.0$ s and $\tau_{s2} = 41.6$ s, for sub-coil 1 and 2, respectively. Here, the influence of the higher resistance in sub-coil 1 can be seen.

V. Conclusion

Our non-insulated VR coil design with iron poles showed its feasibility to reach the nominal performance during powering tests in liquid nitrogen. The VR coil reached the design current of 27 A with a calculated peak field of 0.6 T in the conductor. This was verified via three electrical and thermal cycles. Furthermore, the VR coil showed its quality of being able to transport current up to our test limit, corresponding to 400% of the design current without degradation of the conductor. Additionally, the measured effective time constants of about 42 s and 26 s may be suitable for tunable undulators.

The VR coil will be re-measured at temperatures down to 4.2 K. These tests aim to confirm the potential of coated REBCO conductor tapes, operated at high current densities in the range of 2 kA/mm^2 for wigglers and undulators. This consequently brings peak B-fields on the beam axis in regions of 2.3 T to short periods like 13 mm which no other technology is capable of today. Future investigations of this technology aim for two more single VR prototype coils, including magnetic measurement probes and building a short model.

Acknowledgment

The authors would like to acknowledge C. Fernandes, J. Mazet, F. Garnier, F. O. Pincot, N. Bourcey, S. Clement, P. Martin Vazquez and J. C. Perez for support in the manufacturing process. They would also like to thank G. Lenoir, P. Koziol and C. Barth for supporting the powering tests.

REFERENCES

[1] CompactLight project (XLS). Accessed: Aug. 2021. [Online]. Available: http://www.compact-light.eu/

[2] CLIC study. Accessed: Aug. 2021. [Online]. Available: https://clic.cern/

[3] FCC study. Accessed: Aug. 2021. [Online]. Available: https://fcc.web.cern.ch/

[4] A. Bernhard *et al.*, "A CLIC damping wiggler prototype at ANKA: Commissioning and preparations for a beam dynamics experimental program," in *Proc. IPAC*, 2016, Art. no. WEPMW002.

[5] M. K. Wu *et al.*, "Superconductivity at 93 K in a new mixed-phase Y-Ba-Cu-O compound system at ambient pressure," *Phys. Rev. Lett.*, vol. 58, p. 908, Mar. 1987.

[6] A. Golovashkin *et al.*, "Low temperature direct measurements of Hc_2 in HTSC using megagauss magnetic fields," *Physica C: Supercond.*, vol. 185, pp. 1859–60, Dec. 1991.

[7] G. Brittles and R. Bateman, "Stability and quench—dynamic behaviour of tokamak energy REBCO QA coils," in *Talks at WAMHTS-5*, Budapest, Apr. 2019. Accessed: Aug. 2021. [Online]. Available: https://indico.cern.ch/event/775529/

[8] S. Hahn *et al.*, "45.5-Tesla direct-current magnetic field generated with a high-temperature superconducting magnet," *Nature*, vol. 570, no. 7762, pp. 496–99, Jun. 2019.

[9] I. Kesgin *et al.*, "High-temperature superconducting undulator magnets," *Supercond. Sci. Technol.*, vol. 30, no. 4, Feb. 2017, Art. no. 04LT01.

[10] T. Holubek *et al.*, "A novel concept of high temperature superconducting undulator," *Supercond. Sci. Technol.*, vol. 30, no. 11, Sep. 2017, Art. no. 115002.

[11] C. Boffo and T. Gerhard, "High-temperature superconductor magnet system," Patent WO 2012/013205 Germany, 2012.

[12] M. Calvi *et al.*, "A GdBCO bulk staggered array undulator," *Supercond. Sci. Technol.*, vol. 33, no. 1, Dec. 2020, Art. no. 014004.

[13] S. Richter *et al.*, "High-temperature superconducting undulators for compact free electron lasers," *Proc. German Phys. Soc.*, vol. 50, no. 14, 2019.

[14] F. Nguyen *et al.*, "XLS deliverable D5.1 – Technologies for the compactlight undulator," 2019, Accessed: Aug. 2021. [Online]. Available: https://www.compactlight.eu/Main/Publications

[15] Opera, "Simulation software," 2020. [Online]. Available: https://www.3ds.com/de/produkte-und-services/simulia/produkte/opera/

[16] J. Fleiter and A. Ballarino, "Parameterization of the critical surface of REBCO conductors from Fujikura," *Internal Note*, CERN, Sep. 2014.

[17] M. Danial and J. van Nugteren, "Parameterization of the critical surface of REBCO conductors from Bruker," *Internal Report*, CERN, Jul. 2017.

[18] ANSYS, Inc. Canonsburg, PA, USA, Ansys 19.1 [Online]. Available: https://www.ansys.com/

[19] C. Barth, G. Mondonico, and C. Senatore, "Electro-mechanical properties of REBCO coated conductors from various industrial manufacturers at 77 K, self-field and 4.2 K, 19 T," *Supercond. Sci. Technol.*, vol. 28, no. 4, Feb. 2015, Art. no. 045011.

[20] S. Casalbuoni *et al.*, "Performance of a full scale superconducting undulator with 20 mm period length at the KIT synchrotron," in *Proc. 9th Int. Part. Accel. Conf.*, Vancouver, BC, Canada, Apr. 2018, pp. 4223–4225.

[21] J. Fleiter and A. Ballarino, "In-field electrical resistance at 4.2 K of REBCO splices," *IEEE Trans. Appl. Supercond.*, vol. 27, no. 4, Jun. 2017, Art. no. 6603305.